Published in final edited form as:
Cancer Res. 2011 December 15; 71(24): 7537–7546. doi:10.1158/0008-5472.CAN-11-2170.

Autophagy Enhanced by Microtubule and Mitochondrion-associated MAP1S Suppresses Genome Instability and Hepatocarcinogenesis

Rui Xie[1], **Fen Wang**[1], **Wallace L. McKeehan**[1], and **Leyuan Liu**[1]
[1]Center for Cancer and Stem Cell Biology, Institute of Biosciences and Technology, Texas A&M Health Science Center, Houston, Texas 77030, USA

Abstract

Dysfunctional autophagy is associated with tumorigenesis, yet the relationship between the two processes remains unclear. Here, we show that MAP1S levels immediately become elevated in response to diethylnitrosamine-induced or genome instability-driven metabolic stress in a murine model of hepatocarcinoma. Upregulation of MAP1S enhanced autophagy to remove aggresomes and dysfunctional organelles that trigger DNA double strand breaks and genome instability. The early accumulation of an unstable genome prior to signs of tumorigenesis suggested that genome instability caused tumorigenesis. After tumorigenesis, tumor development then triggered the activation of autophagy to reduce genome instability in tumor foci. We therefore conclude that an increase in MAP1S levels triggers autophagy in order to suppress genome instability, so that both the incidence of diethylnitrosamine-induced hepatocarcinogenesis and malignant progression are suppressed. Taken together, the data establish a link between MAP1S-enhanced autophagy and suppression of genomic instability and tumorigenesis.

Introduction

Autophagy, or self-digestion, is a process that begins with the formation of isolation membranes that engulf substrates such as aggregated proteins or damaged organelles to form autophagosomes. During different stages of cell cycle, cells normally retain robust autophagic activity to remove aggregated proteins or damaged organelles such as mitochondria to maintain cellular hemostasis (1). Under nutritive stresses, autophagy is activated to digest cellular organelles or protein aggregates and recycle the basic components for survival (2). An over-activated autophagy causes organellar depletion and type II program cell death (3). If the autophagic process is blocked before autophagosomal formation, the fragmented mitochondria will release cytochrome *c* and other small molecules to induce conventional apoptosis (4). If autophagosomes are not degraded efficiently, accumulated mitochondria may become damaged by their own production of superoxide and start to leak electrons and lose their membrane potentials. Thus, diverse forms of aggregation and perinuclear clustering of mitochondria are formed and further induce robust oxidative stress that also might trigger apoptotic cell death (5). Therefore, autophagy not only promotes survival but also control cell death. Although a link between

Corresponding Author: Leyuan Liu, Center for Cancer and Stem Cell Biology, Institute of Biosciences and Technology, Texas A&M Health Science Center, Houston, Texas 77030, USA. Phone: 713-677-7518; Fax: 713-677-7512; lliu@ibt.tamhsc.edu.

Findings establish a link between the regulation of autophagy and the suppression of genomic instability and carcinogenesis in a murine model of liver cancer, which is mediated by MAP1S.

Disclosure of Potential Conflicts of Interest
No potential conflicts of interest were disclosed.

autophagic malfunction and cancer was established (6-11), the mechanism by which autophagy suppresses tumorigenesis remains largely unknown (2).

MAP1S was originally described and named as chromosome 19 open reading frame 5 (C19ORF5) (12, 13). It is a widely-distributed homologue of neuronal-specific MAP1A and MAP1B (13, 14). Similar to MAP1A/B, full length MAP1S (MAP1SFL) gives rise to multiple post-translationally modified isoforms including heavy chain (HC) and light chain (LC). Prolonged mitotic arrest or inhibition of the 26S proteasome causes accumulation of an otherwise highly labile short chain (SC) of MAP1S (15, 16). In collaboration with LRPPRC that associates with mitochondria and interacts with Parkinson's disease-related mitophagy initiator Parkin, RASSF1A that is a tumor suppressor and microtubular stabilizer, and LC3 that associates with isolation membrane (12, 13, 16, 17), MAP1S bridges autophagic components with microtubules and mitochondria to affect autophagosomal biogenesis and degradation (16). Ablation of the *Map1s* gene in mice causes impairment in both basal autophagy for clearance of abnormal mitochondria and nutritive stress-induced autophagy for nutrient recycling (16). The MAP1SSC associates with mitochondria in addition to microtubules and causes irreversible aggregation of dysfunctional mitochondria resulting in mitotic cell death (15). Therefore, the MAP1S-depleted mice serve as a good model to test the relationship between autophagy and tumorigenesis.

We show here that in response to the acute increase of oxidative stress imposed by exposure to a chemical carcinogen diethylnitrosamine, MAP1S levels in mouse livers are dramatically elevated to a peak within one day and then decrease to an undetectable level two days after exposure. The acute elevation of MAP1S levels in mouse livers upon diethylnitrosamine exposure leads to activation of autophagy. Activated autophagy leads to removal of P62-associated aggresomes and dysfunctional mitochondria and reduction of DNA double strand breaks (DSB) and genome instability. Because of the ineffective autophagy machinery in the absence of MAP1S, the MAP1S-depleted mice accumulate higher levels of the P62 and γ-H_2AX-marked genome instability even after the acute effect of diethylnitrosamine exposure diminishes two days later. Such higher levels of genome instability than wildtype remain in the livers of diethylnitrosamine-treated adult MAP1S-depleted mice. After tumor foci are detectable in wildtype, MAP1S levels once again shift to high levels in tumor foci but remain undetectable in their adjacent non-tumor tissues. Elevated levels of MAP1S in tumor foci lead to reactivation of autophagy, further leading to reduction of genomic instability within the tumor foci. Because of higher levels of genome instability in liver tissues before tumorigenesis and tumor foci after formation, the MAP1S-depleted mice develop more tumor foci and those benign adenomas are faster to become more malignant hepatocarcinomas. This is the first report from in vivo studies to show a relationship between the autophagy-suppressed oxidative stress and genome instability-driven tumorigenesis from the earliest origin to the latest stage of tumorigenesis.

Materials and Methods

Reagents and antibodies

Antibody against MAP1S (4G1) recognizing an epitope between human MAP1S sequence D667 to S767 was from A&G Pharmaceutical, Inc., Columbia, MD (14, 16). Primary antibodies against β-actin, phosphrylated-H3, FITC- and Rhodamine-conjugated secondary antibodies were from Santa Cruz Biotechnology, Inc., Santa Cruz, CA. Antibody against P62 (SQSTM1) (rabbit polyclonal, BML-PW9860) was from Enzo Life Sciences International, Inc., Plymouth Meeting, PA. Antibody against γ-H_2AX (rabbit polyclonal, A300-081A) was from Bethyl Laboratories, Inc., Montgomery, TX. HRP-conjugated secondary antibodies were from Bio-Rad, Hercules, CA. Diethylnitrosamine (DEN) was

from Sigma-Aldrich, St. Louis, MO. The ECL plus western blotting detection system were from GE Healthcare Biosciences, Pittsburgh, PA.

Analysis of diethylnitrosamine-induced hepatocarcinogenesis in mice

Wildtype and MAP1S-depleted mice were created as described (16) and housed in a pathogen-free animal facility under a standard 12-h light/12-h dark cycle with ad libitum water and chow. Animal protocols were approved by the Institutional Animal Care and Use Committee, Institute of Biosciences and Technology, Texas A&M Health Science Center. Hepatocarcinogenesis were induced with hepatocarcinogen diethylnitrosamine as described (18). Briefly, cohorts of male 15-day-old wildtype and MAP1S-depleted littermates were subjected to a single intraperitoneal administration of 10 μg/g body weight of the diethylnitrosamine dissolved in saline. Mice were sacrificed with euthanasia techniques at 4, 6, 8, 10, and 12 months after birth. Immediately after euthanasia, whole body weights were recorded and the livers were excised, weighed and photographed. Grossly visible surface liver tumors were scored from the top and bottom of each liver. Large macroscopic lesions and their adjacent normal tissues were dissected out. Tissues were either fixed or frozen in liquid nitrogen immediately and stored at –80°C following standard protocols.

Immunoblot, immunostaining and fluorescent confocal microscopy

Lysates from normal liver tissues or tumor samples were prepared and immunoblot was performed as described (16). Immunostaining was performed on 5 μm sections mounted on Superfrost Plus slides (Fisher Scientific, Pittsburgh, PA). Sections were deparaffinized in xylenes and rehydrated through a graded series of ethanol/water solutions. The antigens were retrieved by boiling in citrate buffer (10 mM sodium citrate sodium buffer, pH 6.0) for 20 minutes at 100°C or as suggested by manufacturers of the antibodies. The specifically bound antibodies were detected with fluorescent-conjugated secondary antibody, or HRP-conjugated secondary antibody and visualized using TSA™ Plus Fluorescence System. The sections were counterstained with TOPRO-3 iodide to label nuclei and observed under a Zeiss LSM 510 confocal microscope.

To observe autophagosomes *in vivo*, mouse liver tissues were harvested, frozen and cryosectioned. As reported (16), the GFP-LC3 distribution in frozen sections was directly observed and recorded by fluorescent confocal microscopy. The acquired images were converted to 8-bit binary files, and the number, size and total occupied area of GFP-LC3 punctate foci greater than four pixels in diameter on each image were calculated by ImageJ software.

Partial hepatectomy and liver regeneration

Liver regeneration induced by partial hepatectomy and subsequent analysis were done as described previously (19). Briefly, two third of the liver was surgically removed from 1.5-month-old male mice (20). Mice were sacrificed 48 hrs later. Samples were collected from the regenerated liver tissues and processed for analyses.

Isolation of liver nuclei and flow cytometry analysis

Male mice of indicated age were sacrificed by cervical dislocation. Their livers were rapidly removed and frozen in the liquid nitrogen. The frozen livers were thawed and used to isolate nuclei as described (21). For flow cytometry analysis, the nuclei pellet was resuspended in PI buffer (50 μg/ml Propidium Iodide (PI) and 10 μg/ml RNAse in PBS). The resuspended nuclei was set for 30 minutes at 4°C and analyzed by flow cytometry. The individual profiles of each type of mice were superimposed with each other and DNA contents at 2N peaks were measured. The number of nuclei under each peak of 2-8N was counted.

Results

Depletion of MAP1S gene accelerates diethylnitrosamine-induced hepatocarcinogenesis in mice

To investigate the tumor suppression function of *MAP1S* gene, we set up pairs of wildtype and MAP1S-depleted mice under identical condition without carcinogen and observed for tumorigenesis in all of organs. No abnormality associated with the onset of neoplasia was detected up to 12-month-old. For example, liver tissues of MAP1S-depleted mice were as healthy as those of wildtype mice (Fig. 1A and B). We reasoned that depletion of MAP1S may not be able to initiate tumorigenesis but presence of MAP1S may suppress tumorigenesis induced under certain types of stresses.

We started to induce hepatocarcinogenesis with diethylnitrosamine, a specific initiator of hepatocyte carcinogenesis.(18) Littermates of wildtype (+/+) and MAP1S-depleted mice (-/-) were subjected to a single dose of diethylnitrosamine injection at postnatal 15 days when their livers underwent active proliferation. Their livers reached the full sizes of mature livers about two weeks later. We observed for hepatocarcinogenesis and found tumor foci in MAP1S-depleted liver tissues 6 months and wildtype liver tissues 8 months after birth (Fig. 1A and B). Histologically, the tumor foci were primarily hepatocellular adenomas that caused compression but no disruption of the surrounding normal tissue (Fig. 1C). When mice became older, their body weights were not significantly changed, but tumor incidence, average number of surface tumors per mouse and ratio of liver weight to body weight (LW/BW) were gradually increased. The MAP1S-depleted mice had significantly higher tumor incidence, average number of surface tumors per mouse and ratio of liver weight to body weight (LW/BW) than wildtype mice at the same ages (Fig. 1A, B, D and E). Therefore, *MAP1S* is a tumor suppression gene.

Further detailed examination revealed that hepatocellular carcinoma (HCC) was detected 10 months after birth (Fig. 1A and B). The typical trabecular hepatocarcinomas (HCC) coexisted with the lipid droplet-containing adenomas in aged mice (Fig. 1F), but the MAP1S-depleted mice displayed higher incidence of HCC than the wildtype (Fig. 1A, B and G). Depletion of *MAP1S* gene not only promoted the initiation of tumor foci but also accelerated the conversion of hepatocellular adenomas to malignant hepatocarcinomas.

Acute elevation of MAP1S levels immediately upon exposure to diethylnitrosamine leads to activation of autophagy and reduction of DNA DSB

Although the mechanism is not clearly deciphered, autophagy has been suggested to reduce chromosomal instability and suppress tumorigenesis through elimination of P62-associated aggregated proteins (7, 8). We attempted to deduce a role of MAP1S-regulated autophagy in tumor suppression. The expression levels of MAP1S in normal hepatocytes were too low to be detected by immunoblotting, but dramatically elevated immediately upon exposure to diethylnitrosamine, and then reduced to an undetectable level 2 days after exposure to diethylnitrosamine (Fig. 2A). Our previous results have suggested that MAP1S levels increase upon autophagic activation (16). The wildtype accumulated fewer autophagosomes labeled with GFP-LC3 punctate foci in hepatocytes than MAP1S-depleted mice (Fig. 2B and C), suggesting the acute elevation of MAP1S caused activation of both autophagy initiation and autophagosomal degradation. Examination of LC3-II levels representing a balance of autophagosomal generation and degradation at each sampling point in detail revealed that acute elevation of MAP1S upon diethylnitrosamine exposure enhanced both events but still did not efficiently process all autophagosomes so that certain amount of autophagosomes accumulated and reached a peak at 12 hours. The MAP1S-deficient mice may generate autophagosomes slowly so that LC3-II levels reached a peak at least 12 hours later than the

wild type mice, and also less efficiently remove autophagosomes through lysosomes so that LC3-II levels dropped to base levels five days later than the wild type (Fig. 2A and D).

MAP1S and GFP-LC3 signals distributed in cells mutually exclusively, suggesting that autophagosomes had been degraded efficiently in cells with elevated levels of MAP1S. About 40% of cells had enhanced levels of MAP1S and activated autophagy to degrade autophagosomes while other 60% cells did not increase levels of MAP1S to degrade autophagosomes. More than 80% of hepatocytes accumulated autophagosomes in the MAP1S-depleted mice (Fig. 2E and F), further confirming the role of MAP1S in autophagy. Because of active autophagy, the wildtype hepatocytes were able to efficiently eliminate the P62-associated aggresomes and dysfunctional organelles. Two weeks after exposure, levels of P62 reduced to levels close to but still higher than the ones before exposure. In contrast, the MAP1S-deficient hepatocytes maintained higher levels of P62 than the wild type (Fig. 2A and D). Therefore, elevated levels of MAP1S lead to activation of autophagy to reduce the diethylnitrosamine-induced aggresomes and dysfunctional organelles.

Protein aggresomes and dysfunctional organelles such as mitochondria and endoplasm reticulum induce oxidative stress that causes DNA DSB and genome instability (7, 8, 22). Intensity of DNA DSB is represented by the levels of phosphorylated H2AX (γ-H_2AX) (23). No DNA DSB labeled with γ–H_2X was found in untreated hepatocytes of both wildtype and MAP1S-depleted mice (Fig. 2G). Along with the acute elevation of MAP1S levels, DNA DSB was also dramatically intensified immediately upon exposure to diethylnitrosamine (Fig. 2A, D and H). Similar to the mutually exclusive distribution of GFP-LC3 punctate foci and MAP1S signals, MAP1S levels were lower in the cells with DNA DSB (Fig. 2G). The MAP1S-depleted mice exhibited higher levels of DNA DSB in hepatocytes immediately upon diethylnitrosamine treatment and maintained higher levels than the wildtype until livers were fully matured two weeks after diethylnitrosamine treatment (Fig. 2A, D and H). Therefore, depletion of *MAP1S* gene impaired normal autophagy function, leading to accumulation of higher levels of genome instability that increase the chance to form tumor foci in future.

The diethylnitrosamine-induced DNA DSB and genome instability that persist in the adult liver tissues are suppressed by MAP1S

It is well-known that chromosomal fragments with DSB tend to randomly fuse either correctly with the original broken chromosomal fragment or erroneously with fragment broken from other chromosome. The erroneously ligated chromosome undergoes breakage-fusion-bridge cycles in successive mitoses that eventually lead to chromosome instability (24). Majority of hepatocytes with DNA DSB upon diethylnitrosamine treatment had their broken ends fused that no γ–H_2X signal was readily to be detected one month after exposure to diethylnitrosamine. We reasoned that those hepatocytes still generate daughter cells with DNA DSB because of the breakage-fusion-bridge mechanism. However, nearly no mitotic hepatocyte was able to be identified in the adult livers (Fig. 3A) so that it was technically hard to test the hypothesis. To increase mitotic index, we conducted partial hepatectomy to induce liver regeneration in 2 month-old mice, which led to dramatic increase of number of mitotic hepatocytes (Fig. 3A).

Both normal and diethylnitrosamine-treated mitotic hepatocytes were driven into mitosis during liver regeneration. The untreated mitotic hepatocytes exhibited no DNA DSB, while mitotic hepatocytes that had exposed to diethylnitrosamine one and half months ago contained large number of DNA DSB (Fig. 3B). The DNA DSB signals were clearly overlapped with the condensed chromosomes in those mitotic hepatocytes (Fig. 3C). Relatively, fewer mitotic hepatocytes carried DNA DSB in the wildtype than in the MAP1S-depleted mice (Fig. 3B and D). Although partial hepatectomy created a highly artificial and

unexpected biological condition, the results suggested that hepatocytes in diethylnitrosamine-treated MAP1S-depleted mice had higher chance than the wildtype to generate daughter hepatocytes with genome instability if they had chance to re-enter mitosis.

We further examined the livers of four-month-old diethylnitrosamine-treated mice and found no tumor focus in either wildtype or MAP1S-depleted mice (Fig. 1A). Constant evolution of the destabilized genomes during the three and half months after exposure to diethylnitrosamine might lead to preservation of DNA DSB although no tumor focus was detectable. The MAP1S-depleted mice contained slightly but significantly higher levels of DNA DSB in livers that did not developed into any detectable tumor focus yet (Fig. 4A and B). Examination of DNA contents by flow cytometry revealed that hepatocytes from both wildtype and the MAP1S-depleted mice contained amounts of genomic DNA that were deviated from their normal 2N DNA content (Fig. 4C). The depletion of *MAP1S* gene caused a wider range of variation of 2N DNA contents (Fig. 4C and D) and higher percentage of polyploidy hepatocytes (Fig. 4C and E). Polyploidy cells often lead to generation of aneuploidy and genome instability during proliferation because of weakened mitotic checkpoint (25). Thus, the knockout mice had higher levels of tumorigenesis-driving genome instability.

Elevation of MAP1S levels within tumor foci of diethylnitrosamine-treated mice leads to activation of autophagy influx and reduction of DNA DSB

The persistence of higher genomic instability in the MAP1S-depleted hepatocytes represented a higher chance of tumorigenesis, which explains why the MAP1S-depleted mice had higher tumor incidence and more surface tumors than the wildtype. The reason that the MAP1S-depleted mice developed more malignant HCC was still not explained. We measured the MAP1S levels adenomas of similar sizes in diethylnitrosamine-treated 10-month-old mouse livers. The levels of MAP1S were undetectable in non-tumor adjacent liver tissues from wildtype mice, and similar to the levels in liver tissues of untreated mice (Fig. 2A), but dramatically elevated in majority of tumor foci (Fig. 5A, B and C). It was likely that such increase was caused by metabolic stresses resulted from genome instability.

Cells in the aged livers contained different genomes among different individuals (Fig. 4C and D). Each diversified genome evolves and adopts a different set of autophagy machinery. Under such condition, the LC3-II levels may represent balances of different generation and degradation rates. As expected, the LC3-II levels were not significantly different between tumor foci and neighboring tissues, and between wildtype and MAP1S-deficient mice (Fig. 5C, and D). However, high levels of MAP1S indicate activation of autophagy influx leading to reduction of autophagy substrates (16). More P62-associated protein aggregates and dysfunctional organelles accumulated in MAP1S-deficient tumor foci (Fig. 5C, E and F), suggesting dramatic reduction of autophagy influx. The increase of MAP1S levels leads to increase of autophagy influx and reduction of P62 levels in the diethylnitrosamine-induced tumor foci of wildtype livers. The deficiency in autophagic response in the tumor foci of the MAP1S-depleted livers reflected by such accumulation correspondingly led to increase of DNA DSB (Fig. 5C, G and H). Higher degree of genomic instability in the tumor foci led to development of more malignant HCC. Thus, an active autophagy suppressed genome instability in tumor foci so that less malignant tumor was developed.

Discussion

Chromosomal instability, as the most common type of genome instability, mainly results from either whole chromosome aneuploidy due to mitotic errors or segmental aneuploidy due to chromosomal rearrangements including deletions, amplifications or translocation (26). Although aneuploidy is not synonymous with chromosomal instability (26),

aneuploidy was suggested to be the origin of tumorigenesis (27). Since then, it has been hotly debated whether point mutation or genomic instability is the cause or the consequence of tumorigenesis (28). Our results indicate that early before tumorigenesis, significant levels of genomic instability exist in the liver tissues exposure to the chemical carcinogen diethylnitrosamine. This suggests that that genomic instability may be the cause of hepatocarcinogenesis. The positive co-relationship between genomic instability and malignancy of tumor foci as revealed in this study further suggests that genomic instability is also the driving force of cancer development. Thus, high levels of genomic instability provide high chances of tumor initiation and wide genetic variation to evolve into high malignant tumor foci.

An inverse relationship between autophagic activity and malignant transformation has been established since 1999 (29). A high incidence of spontaneous tumors in systemic mosaic deletion of ATG5, ATG7$^{-/-}$, Beclin 1$^{+/-}$ and Beclin 1-interactive protein Bif-1$^{-/-}$ mutant mice enforced a role of autophagy in tumor suppression (6, 10, 11, 30). The ATG4C-depleted mice show an increased susceptibility to develop fibrosarcomas induced by chemical carcinogens (9). Similarly, the MAP1S-depeleted mice have demonstrated a suppressive role in diethylnitrosamine-induced hepatocarcinomas. The contradiction suggests that ATG5, ATG7, Beclin 1 and Bif-1 may play roles in addition to autophagic regulation.

In order to understand the relationship between autophagy and tumor suppression, a link through P62 and γ-H_2AX has been well established (7, 8). P62, or Sequestosome 1, associates with ubiquitin-positive Mallory-Denk bodies in hepatocytes of patients with alcoholic hepatitis and a variety of other liver diseases (31). P62 protein serves as receptor to bind with ubiquitinated substrates such as aggregated proteins and dysfunctional organelles including mitochondria for autophagosomal biogenesis, and its levels represent the amount of aggregated proteins and dysfunctional organelles accumulated in cells (32). Balanced autophagy aids cells in clearance of aggregated proteins and dysfunctional organelles and thereby reducing P62 levels that serve as accurate monitors of the intensity of cellular oxidative stress. A defect in autophagy enhances oxidative stress resulting in cell death (7). However, oxidative stress leads to DNA DSB (22, 33, 34) since it can simultaneously subvert mitotic checkpoints (35, 36).

In cytogenetic point of view, a chromosomal fragment with a break tends to randomly fuse with another broken chromosomal fragment, which potentially leads to the formation of a new chromosome with two centromeres if ligation happens between two fragments with centromeres. The cell containing chromosome with two centromeres forms a chromosomal bridge during mitotic metaphase and the resulted chromosomal bridge will break and generate new broken ends after telophase (24, 37). Modern molecular biology suggests that DNA DSB will be repaired through either homologous recombination (HR) or non-homologous end-joining (NHEJ) while NHEJ is believed to be the predominant mechanism of DSB repair in higher eukaryotes (38). Cells with DSBs will experience mitotic defect that will activate mitotic checkpoint and temporally result in mitotic arrest and mitotic cell death (15). If cells can escape the arresting through the so-called mitotic slippage, the resulted aneuploidy daughter cells are generally lethal. Therefore, genome instability is intrinsically tumor suppressive (39). However, if an aneuploidy cell can escape mitotic checkpoint and survive, it potentially initiates a cascade of autocatalytic karyotypic evolution through the continuous cycles of chromosomal breakage-fusion-bridge and eventually destabilizes the genome. A destabilized genome results in either inactivation of tumor suppressor genes or activation of oncogenes through point mutation, rearrangement of wildtype genes in new locations on genome to play malfunctions, or creation of fusion gene between different wildtype genes to play new function. Such genetic variation generates the opportunity for phenotypic selection which results in continuous evolution and diversity of cancer

phenotypes during the progression (24, 28, 40). Thus, autophagic defect-resulted oxidative stress could either suppress tumorigenesis if it can trigger cell death or promote tumorigenesis if the cells can survive the insult of oxidative stress.

It has been known that animals exposed to diethylnitrosamine exhibit increased levels of oxidative stress (41). We believe such increase in oxidative stress may be caused by accumulation of P62-associated protein aggresomes and dysfunctional organelles. We knew that MAP1S positively regulates autophagic activity and its increase upon diethylnitrosamine exposure indicates an autophagic activation. Activated autophagy leads to removal of P62 and reduction of oxidative stress while the animals with defective autophagy accumulate high levels of P62 and oxidative stress. MAP1S-activated autophagy causes reduction of both oxidative stress and genomic instability immediately upon diethylnitrosamine exposure. The MAP1S-depleted mice accumulate higher levels of genomic instability and have higher probability to generate tumor progenitor cells that will be developed into visible tumor foci several months later. In order for the tumor progenitor cells to evolve into large tumor foci, cells continue multiple rounds of mitoses that will further destabilize the genome and results in accumulation of oxidative stress (42). Such stress will reactivate MAP1S-regulated autophagic machinery and in turn reduce the levels of P62 and oxidative stress. The inactive autophagy in MAP1S-depleted mice causes accumulation of P62, oxidative stress and genomic instability in tumor foci. Mice with destabilized genome will lead to develop high malignant hepatocarcinomas. The high incidence of tumor foci and hepatocarcinomas in the MAP1S-depleted mice clearly attest that MAP1S suppress hepatocarcinogenesis through autophagy regulation.

Acknowledgments

We thank Dr. Le Sun and Joe Corvera (A&G Pharmaceuticals, Inc., Columbia, MD) for anti-MAP1S mouse monoclonal antibody 4G1 which is now sold by Precision Antibody™ with catalog number of AG10006. LC3 cDNA and GFP-LC3 transgenic mice were gifts from Dr. Noboru Mizushima, Department of Physiology and Cell Biology, Tokyo Medical and Dental University Graduate School and Faculty of Medicine. Ms. Susan Nguyen and Kerstin McKeehan provided excellent technical assistance.

Grant Support

This work was supported by DOD New Investigator Award W81XWH (LL), NCI 1R01CA142862 (LL), NCI P50 CA140388 (WLM), the Susan Komen Foundation (WLM), and aid from the John S. Dunn Research Foundation (WLM).

References

1. Liu L, Xie R, Nguyen S, Ye M, McKeehan WL. Robust autophagy/mitophagy persists during mitosis. Cell Cycle. 2009; 8:1616–20. [PubMed: 19411827]
2. Mizushima N, Levine B, Cuervo AM, Klionsky DJ. Autophagy fights disease through cellular self-digestion. Nature. 2008; 451:1069–75. [PubMed: 18305538]
3. Kroemer G, Jaattela M. Lysosomes and autophagy in cell death control. Nat Rev Cancer. 2005; 5:886–97. [PubMed: 16239905]
4. Desagher S, Martinou JC. Mitochondria as the central control point of apoptosis. Trends Cell Biol. 2000; 10:369–77. [PubMed: 10932094]
5. Boya P, Gonzalez-Polo RA, Casares N, Perfettini JL, Dessen P, Larochette N, et al. Inhibition of macroautophagy triggers apoptosis. Mol Cell Biol. 2005; 25:1025–40. [PubMed: 15657430]
6. Qu X, Yu J, Bhagat G, Furuya N, Hibshoosh H, Troxel A, et al. Promotion of tumorigenesis by heterozygous disruption of the beclin 1 autophagy gene. J Clin Invest. 2003; 112:1809–20. [PubMed: 14638851]
7. Mathew R, Karp CM, Beaudoin B, Vuong N, Chen G, Chen HY, et al. Autophagy suppresses tumorigenesis through elimination of p62. Cell. 2009; 137:1062–75. [PubMed: 19524509]

8. Mathew R, Kongara S, Beaudoin B, Karp CM, Bray K, Degenhardt K, et al. Autophagy suppresses tumor progression by limiting chromosomal instability. Genes Dev. 2007; 21:1367–81. [PubMed: 17510285]
9. Marino G, Salvador-Montoliu N, Fueyo A, Knecht E, Mizushima N, Lopez-Otin C. Tissue-specific autophagy alterations and increased tumorigenesis in mice deficient in Atg4C/autophagin-3. J Biol Chem. 2007; 282:18573–83. [PubMed: 17442669]
10. Yue Z, Jin S, Yang C, Levine AJ, Heintz N. Beclin 1, an autophagy gene essential for early embryonic development, is a haploinsufficient tumor suppressor. Proc Natl Acad Sci U S A. 2003; 100:15077–82. [PubMed: 14657337]
11. Takahashi Y, Coppola D, Matsushita N, Cualing HD, Sun M, Sato Y, et al. Bif-1 interacts with Beclin 1 through UVRAG and regulates autophagy and tumorigenesis. Nat Cell Biol. 2007; 9:1142–51. [PubMed: 17891140]
12. Liu L, Amy V, Liu G, McKeehan WL. Novel complex integrating mitochondria and the microtubular cytoskeleton with chromosome remodeling and tumor suppressor RASSF1 deduced by in silico homology analysis, interaction cloning in yeast, and colocalization in cultured cells. In Vitro Cell Dev Biol Anim. 2002; 38:582–94. [PubMed: 12762840]
13. Liu L, McKeehan WL. Sequence analysis of LRPPRC and its SEC1 domain interaction partners suggest roles in cytoskeletal organization, vesicular trafficking, nucleocytosolic shuttling and chromosome activity. Genomics. 2002; 79:124–36. [PubMed: 11827465]
14. Liu L, Vo A, Liu G, McKeehan WL. Distinct structural domains within C19ORF5 support association with stabilized microtubules and mitochondrial aggregation and genome destruction. Cancer Res. 2005; 65:4191–201. [PubMed: 15899810]
15. Liu L, Xie R, Yang C, McKeehan WL. Dual function microtubule- and mitochondria-associated proteins mediate mitotic cell death. Cell Oncol. 2009; 31:393–405. [PubMed: 19759419]
16. Xie R, Nguyen S, McKeehan K, Wang F, McKeehan WL, Liu L. Microtubule-associated Protein 1S (MAP1S) Bridges Autophagic Components with Microtubules and Mitochondria to Affect Autophagosomal Biogenesis and Degradation. J Biol Chem. 2011; 286:10367–77. [PubMed: 21262964]
17. Davison EJ, Pennington K, Hung CC, Peng J, Rafiq R, Ostareck-Lederer A, et al. Proteomic analysis of increased Parkin expression and its interactants provides evidence for a role in modulation of mitochondrial function. Proteomics. 2009; 9:4284–97. [PubMed: 19725078]
18. Huang X, Yang C, Jin C, Luo Y, Wang F, McKeehan WL. Resident hepatocyte fibroblast growth factor receptor 4 limits hepatocarcinogenesis. Mol Carcinog. 2009; 48:553–62. [PubMed: 19009564]
19. Huang X, Yu C, Jin C, Kobayashi M, Bowles CA, Wang F, et al. Ectopic activity of fibroblast growth factor receptor 1 in hepatocytes accelerates hepatocarcinogenesis by driving proliferation and vascular endothelial growth factor-induced angiogenesis. Cancer Res. 2006; 66:1481–90. [PubMed: 16452204]
20. Mitchell C, Willenbring H. A reproducible and well-tolerated method for 2/3 partial hepatectomy in mice. Nat Protoc. 2008; 3:1167–70. [PubMed: 18600221]
21. Ho YF, Guenthner TM. Isolation of liver nuclei that retain functional trans-membrane transport. J Pharmacol Toxicol Methods. 1997; 38:163–8. [PubMed: 9523770]
22. Liu L, Trimarchi JR, Smith PJ, Keefe DL. Mitochondrial dysfunction leads to telomere attrition and genomic instability. Aging Cell. 2002; 1:40–6. [PubMed: 12882352]
23. Paull TT, Rogakou EP, Yamazaki V, Kirchgessner CU, Gellert M, Bonner WM. A critical role for histone H2AX in recruitment of repair factors to nuclear foci after DNA damage. Curr Biol. 2000; 10:886–95. [PubMed: 10959836]
24. McClintock B. The Fusion of Broken Ends of Chromosomes Following Nuclear Fusion. Proc Natl Acad Sci U S A. 1942; 28:458–63. [PubMed: 16578057]
25. Storchova Z, Pellman D. From polyploidy to aneuploidy, genome instability and cancer. Nat Rev Mol Cell Biol. 2004; 5:45–54. [PubMed: 14708009]
26. Geigl JB, Obenauf AC, Schwarzbraun T, Speicher MR. Defining ‘chromosomal instability’. Trends Genet. 2008; 24:64–9. [PubMed: 18192061]

27. Boveri, T. Zur Frage der Entstehung maligner Tumoren. Gustav Fischer Verlag; Jena, Germany: 1914.
28. Duesberg P, Rasnick D. Aneuploidy, the somatic mutation that makes cancer a species of its own. Cell Motil Cytoskeleton. 2000; 47:81–107. [PubMed: 11013390]
29. Liang XH, Jackson S, Seaman M, Brown K, Kempkes B, Hibshoosh H, et al. Induction of autophagy and inhibition of tumorigenesis by beclin 1. Nature. 1999; 402:672–6. [PubMed: 10604474]
30. Takamura A, Komatsu M, Hara T, Sakamoto A, Kishi C, Waguri S, et al. Autophagy-deficient mice develop multiple liver tumors. Genes Dev. 2011; 25:795–800. [PubMed: 21498569]
31. Zatloukal K, French SW, Stumptner C, Strnad P, Harada M, Toivola DM, et al. From Mallory to Mallory-Denk bodies: what, how and why? Exp Cell Res. 2007; 313:2033–49. [PubMed: 17531973]
32. Komatsu M, Waguri S, Koike M, Sou YS, Ueno T, Hara T, et al. Homeostatic levels of p62 control cytoplasmic inclusion body formation in autophagy-deficient mice. Cell. 2007; 131:1149–63. [PubMed: 18083104]
33. Marietta C, Thompson LH, Lamerdin JE, Brooks PJ. Acetaldehyde stimulates FANCD2 monoubiquitination, H2AX phosphorylation, and BRCA1 phosphorylation in human cells in vitro: implications for alcohol-related carcinogenesis. Mutat Res. 2009; 664:77–83. [PubMed: 19428384]
34. Mishra PK, Raghuram GV, Panwar H, Jain D, Pandey H, Maudar KK. Mitochondrial oxidative stress elicits chromosomal instability after exposure to isocyanates in human kidney epithelial cells. Free Radic Res. 2009; 43:718–28. [PubMed: 19513903]
35. D'Angiolella V, Santarpia C, Grieco D. Oxidative stress overrides the spindle checkpoint. Cell Cycle. 2007; 6:576–9. [PubMed: 17351333]
36. Li M, Fang X, Baker DJ, Guo L, Gao X, Wei Z, et al. The ATM-p53 pathway suppresses aneuploidy-induced tumorigenesis. Proc Natl Acad Sci U S A. 2010; 107:14188–93. [PubMed: 20663956]
37. Gisselsson D, Pettersson L, Hoglund M, Heidenblad M, Gorunova L, Wiegant J, et al. Chromosomal breakage-fusion-bridge events cause genetic intratumor heterogeneity. Proc Natl Acad Sci U S A. 2000; 97:5357–62. [PubMed: 10805796]
38. Burma S, Chen BP, Chen DJ. Role of non-homologous end joining (NHEJ) in maintaining genomic integrity. DNA Repair (Amst). 2006; 5:1042–8. [PubMed: 16822724]
39. Weaver BA, Cleveland DW. Decoding the links between mitosis, cancer, and chemotherapy: The mitotic checkpoint, adaptation, and cell death. Cancer Cell. 2005; 8:7–12. [PubMed: 16023594]
40. Mitelman F, Johansson B, Mertens F. The impact of translocations and gene fusions on cancer causation. Nat Rev Cancer. 2007; 7:233–45. [PubMed: 17361217]
41. Yamada K, Yamamiya I, Utsumi H. In vivo detection of free radicals induced by diethylnitrosamine in rat liver tissue. Free Radic Biol Med. 2006; 40:2040–6. [PubMed: 16716904]
42. Limoli CL, Giedzinski E, Morgan WF, Swarts SG, Jones GD, Hyun W. Persistent oxidative stress in chromosomally unstable cells. Cancer Res. 2003; 63:3107–11. [PubMed: 12810636]

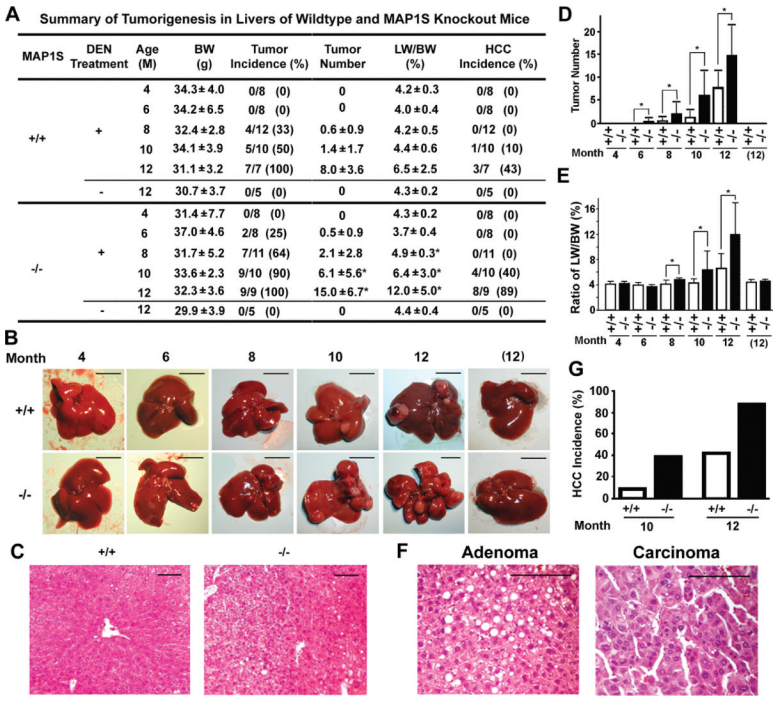

Figure 1.

Depletion of MAP1S promotes diethylnitrosamine-induced hepatocarcinogenesis in mice. A, a summary of tumorigenesis in the liver tissues of wildtype and MAP1S-depleted mice at different times after diethylnitrosamine (DEN) treatment. Data is the mean ± SD of each group and difference was statistically determined by Student's t test. *, $p \leq 0.05$. B., the morphology of livers of diethylnitrosamine-treated wildtype and MAP1S-depleted mice at different ages. (12), 12-month-old without diethylnitrosamine treatment. Bar = 10 mm. C, a comparative H&E staining of livers of diethylnitrosamine-treated 6-month-old wildtype and MAP1S-depletion mice. A normal liver of wildtype mouse is compared to a liver with adenomas of MAP1S-depleted mouse. Bar = 100 μm. D and E, a plot of tumor number (D) or ratio of liver weight to body weight (E) to ages of diethylnitrosamine-treated wildtype and MAP1S-depleted mice as listed in (A). F, a comparative Hematoxylin and Eosin (H&E) staining of livers of diethylnitrosamine-treated 10-month-old wildtype and MAP1S-depleted mice. Bar = 100 μm. G, a plot of hepatocarcinomas (HCC) incidence to ages of wildtype and MAP1S-depleted mice after diethylnitrosamine treatments as listed in (A).

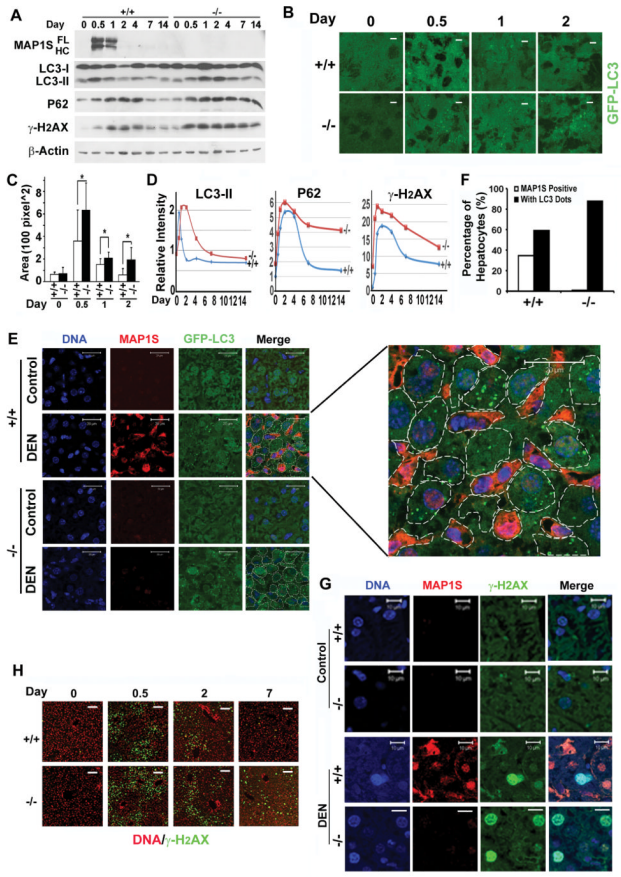

Figure 2.

Acute elevation of MAP1S levels immediately upon diethylnitrosamine exposure leads to activation of autophagy and reduction of DNA DSB. A, an immunoblot analysis of liver lysates from wild-type (+/+) and MAP1S-depleted mice (-/-) injected with diethylnitrosamine (25 μg/g body weight). Liver tissues were collected immediately or at different days after diethylnitrosamine injection. FL, full-length MAP1S; HC, heavy chain of MAP1S. B, representative images showing GFP-LC3 punctate foci appeared in liver tissues at the indicated times after diethylnitrosamine treatment. The *GFP-LC3*$^{+/-}$*MAP1S*$^{-/-}$ mice (-/-) and their *GFP-LC3*$^{+/-}$*MAP1S*$^{+/+}$ controls (+/+) were similarly treated with diethylnitrosamine as in (A). Bar = 100 μm. C, quantitation of the total area of GFP-LC3 punctate foci with size larger than 100 pixel^2. Data is the average and standard deviation of ten randomly selected images in a field of 512 pixel × 512 pixels. The significance of differences was determined by Student's t-test. *, $p<0.05$. D, a plot of relative intensities of P62 and γ-H2AX bands shown in (A) with the value in wild type mice at day 0 as the standard 1. Data is a representative set of three repeats all of which exhibit the same large differences between the wild type and knockout but varied relative intensities due to the varied intensity of the standards. E, relative distribution of GFP-LC3 and MAP1S in liver tissues 12 hr after diethylnitrosamine (DEN) treatment. Tissue sections prepared as in (B) were fixed and subjected to immunostaining. Cell boundaries were outlined with white dot lines. Bar = 20 μm. F, percentage of cells with MAP1S positive signals or GFP-LC3 punctate foci 12 hr after diethylnitrosamine treatment. Samples were prepared and observed as described in (E). Data is the summary of ten randomly selected images containing about 2,000 cells in total. G, relative distribution of MAP1S and γ-H_2AX in liver tissues 12 hr after diethylnitrosamine (DEN) treatment. . Pairs of *MAP1S*$^{+/+}$ (+/+) and *MAP1S*$^{-/-}$mice (-/-)

were similarly treated with diethylnitrosamine as in (A), and liver tissues were fixed and subjected to immune-staining. Bar = 10 μm. H, representative images showing γ–H_2AX signals in liver tissues of *MAP1S*$^{+/+}$ (+/+) and *MAP1S*$^{-/-}$ mice (-/-) at the indicated times after diethylnitrosamine treatment. Nuclei were counter-stained. Bar = 100 μm.

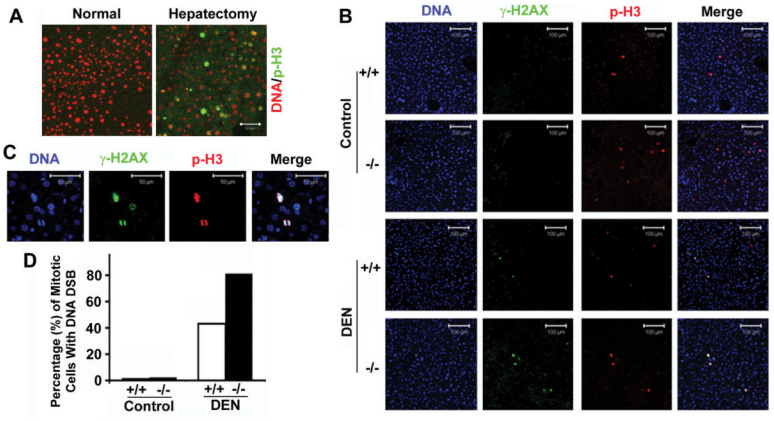

Figure 3.

MAP1S suppresses the diethylnitrosamine-induced DNA DSB and instability that persist in the fully developed liver tissues one month after diethylnitrosamine treatment. A, an immuno-staining analysis showing that partial hepatectomy (PH) reactivates mitosis for liver regeneration. Tissue sections were stained with TOPRO-3 to label nuclei (red) and anti-phosphorylated histone H3 (p-H3) to label mitotic cells (green). Bar = 50 μm. B, representative images showing mitotic cells with DNA DSB in regenerated liver tissues. Liver hepatectomy was performed on both *MAP1S*$^{+/+}$ (+/+) and *MAP1S*$^{-/-}$ mice (-/-) one month after diethylnitrosamine (DEN) treatment to induce hepatocytes proliferation. Status of DNA DSB and cell proliferation were identified by immune-staining with antibody against γ-H_2Ax or p-H3 in addition to DNA stained chromosomes. The untreated mice serve as control. Bar = 100 μm. C, an enlarged image showing mitotic cells with DNA DSB in regenerated liver tissues of MAP1S-depleted mice. Bar = 50 μm. D, the percentage of mitotic cells with DNA double-strand breaks to the total mitotic cells in the regenerated liver tissues after hepatectomy.

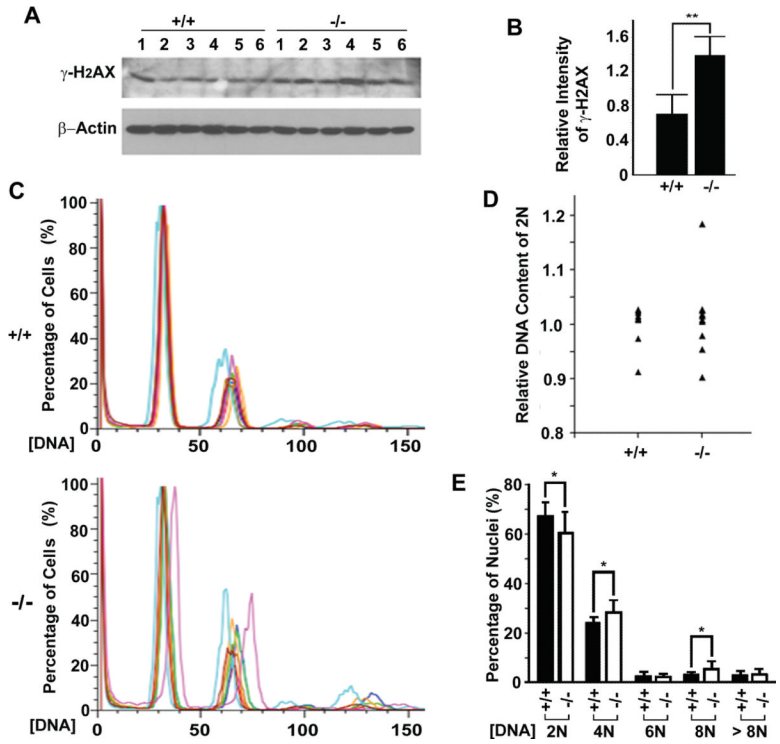

Figure 4.

MAP1S suppresses the diethylnitrosamine-induced DNA DSB and instability that persist in liver tissues from four-month-old diethylnitrosamine-treated mice. A, immunoblot of liver lysates from diethylnitrosamine-treated four-month-old wild-type (+/+) and MAP1S-depleted mice (-/-). Samples were collected from 6 pairs of littermates. B, a plot of relative intensities of γ-H2AX bands shown in (A) with the value in wild type mouse number 1 as the standard 1. Data is the average and standard deviation of 6 mice. The significances of differences between wildtype and knockout mice were determined by Student's t-test. *, $p<0.01$. C, flow cytometric analyses of hepatic nuclei isolated from livers of diethylnitrosamine-treated four-month-old mice that did not exhibit any tumor foci. For each genotype, eight mice were subjected to analysis for their DNA contents by propidium iodide (PI) staining, and their histograms in different colors were superimposed with each other. D, the distribution of relative DNA contents at 2N peaks. The DNA contents of 2N nuclei were quantified from data of eight pairs of mice shown in (C) and normalized with the average contents of all wildtype mice. E, the percentages of nuclei with DNA contents around peaks of 2N, 4N, 6N, 8N and >8N to the total number of nuclei in each sample shown in (C) were quantified. Data is the average and standard deviation of 8 mice. The significances of differences between wildtype and knockout mice were determined by Student's t-test. *, $p<0.05$.

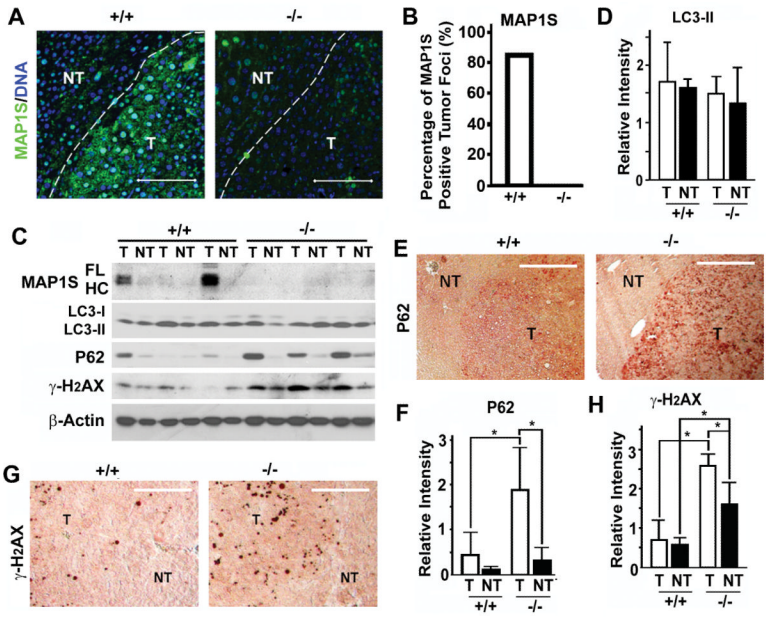

Figure 5.

Elevation of MAP1S levels leads to activation of autophagy influx and reduction of DNA DSB within tumor foci in livers of diethylnitrosamine-treated ten-month-old mice. A, representative images showing the immunostaining patterns of MAP1S in adjacent tumor tissues (T) and normal tissues (NT) from livers of diethylnitrosamine-treated ten-month-old wild-type (+/+) and MAP1S-depleted mice (-/-). All bars in this figure equal to 100 μm. B, a summary of percentage of MAP1S positive tumor foci in livers of wild type (+/+) and MAP1S knockout mice (-/-). About 10 hepatoadenomas were examined for each group. C, immunoblot of lysates from adjacent tumor tissues (T) and normal tissues (NT) isolated from livers of diethylnitrosamine-treated ten-month-old wild-type (+/+) and MAP1S-depleted mice (-/-). The same amount of total proteins was loaded for each lane. D, a plot of relative intensities of LC3-II bands shown in (C) with the value in the first wild type tumor sample as the standard 1. Data is the mean and standard deviation of three repeats. E, representative images showing immunostaining profiles of liver tissues carrying hepatoadenoma with antibody against P62. F, a plot of relative intensities of P62 bands shown in (C) with the value in the first wild type tumor sample as the standard 1. Data is the mean and standard deviation of three repeats. The significances of differences between tumor and adjacent normal tissues and between wildtype and knockout mice were determined by Student's t-test. *, $p<0.05$. G, representative images showing immunostaining profiles of liver tissues carrying hepatoadenoma with antibody against γ-H_2AX. H, a plot of relative intensities of γ-H2AX bands shown in (C). Data was collected and analyzed similarly as in (F).